

Supplemental Material for Glacier projections sensitivity to temperature-index model choices and calibration strategies

LILIAN SCHUSTER¹, DAVID R. ROUNCE², FABIEN MAUSSION^{1,3}

submitted to the Annals of Glaciology

Special Issue: Ice, Snow, Water and Permafrost in a Warming World

Contents

S1 Supplemental Material and Figures for the calibration and model performance	2
S1.1 Temperature-index model choice influence on calibrated parameter combinations (related to Sect. 3.1.1)	3
S1.2 Supplemental Figures of temperature-index model choice and calibration strategy performance (related to Sect. 3.1.3 and Sect. 3.2.2)	4
S1.3 Supplemental Figures of the influence of equifinality on the temperature-index model output (related to Sect. 3.2.1)	7
S2 Supplemental Figures of volume projections (related to Sect. 4)	10
S3 Supplemental Figures of runoff projections (related to Sect. 4)	13
S4 Supplemental Material for the discussion	18
S4.1 Comparison of other studies discussing the added value of more observations for the calibration (related to Sect. 5.1.4)	18

¹Department of Atmospheric and Cryospheric Sciences (ACINN), Universität Innsbruck, Innsbruck, Austria

²Department of Civil and Environmental Engineering, Carnegie Mellon University, Pittsburgh, PA, United States

³School of Geographical Sciences, University of Bristol, Bristol, UK

S1 Supplemental Material and Figures for the calibration and model performance

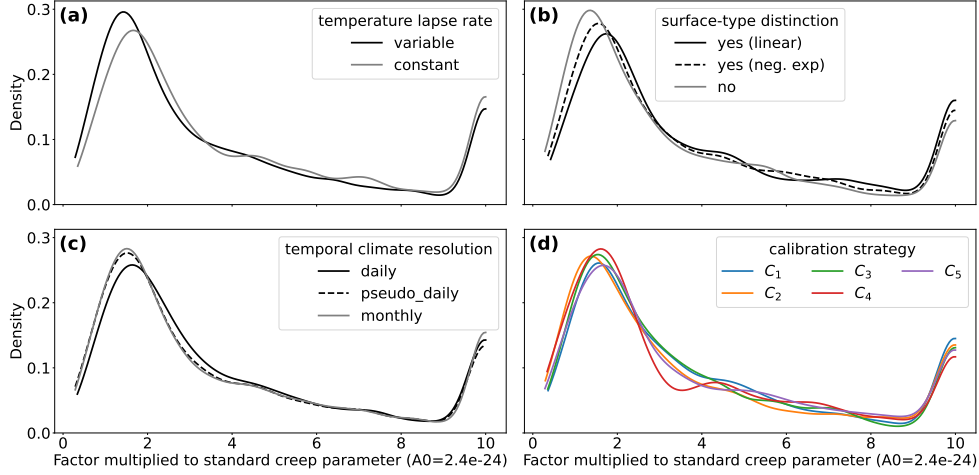


Figure S1: Distributions of calibrated creep parameters to match the consensus volume estimate of Farinotti and others (2019) for each of the 88 glaciers (depicted as kernel density estimates truncated at the data limits). We show the influence of **(a)** temperature lapse rate, **(b)** surface-type distinction **(c)** temporal climate resolution, and **(d)** calibration strategies on the factor that we multiplied to the standard creep parameter (median of 2.6, thresholds set to [0.1, 10]).

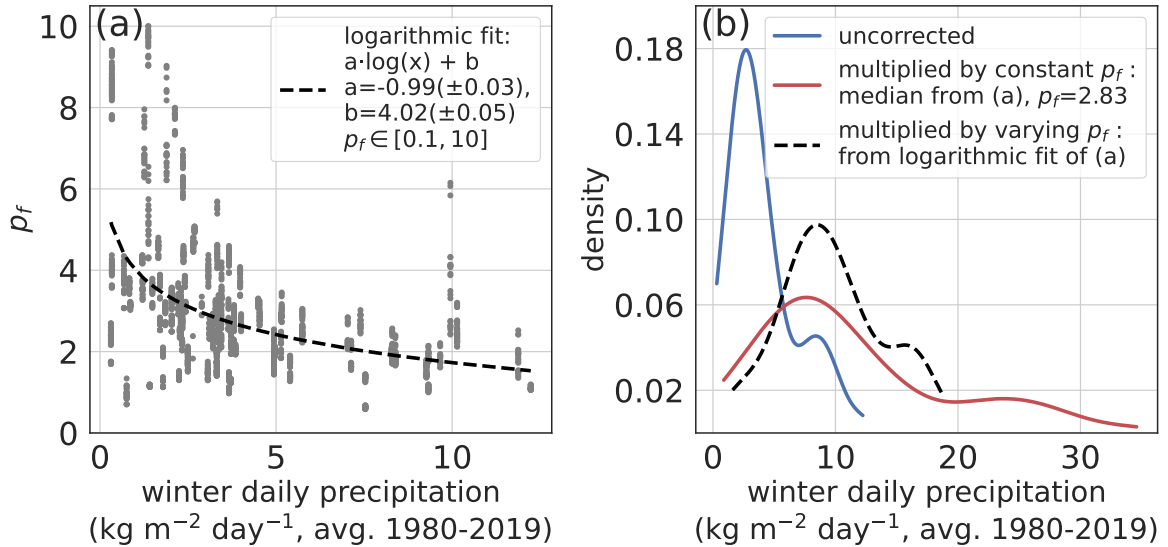


Figure S2: **(a)** Relation between winter daily precipitation and calibrated precipitation factor (p_f) for C_2 for the 114 glaciers where the calibration to match the winter MB was possible for all temperature-index model choices together (correlation coefficient $R^2=0.2$). The logarithmic fit with one standard deviation error of the parameters is given. This relation is used to estimate a glacier-specific p_f for C_5 . The only relation between calibrated p_f and glacier(-climate) characteristic that we found was with winter precipitation (i.e., average daily precipitation over the years 1980–2019 between October and April for glaciers in the Northern Hemisphere and between April and September for glaciers in the Southern Hemisphere). **(b)** Uncorrected and corrected precipitation distributions of the 114 glaciers. If the same p_f , median from (a), is applied to each glacier, the precipitation distribution width is much larger than the uncorrected one or the one using a winter-precipitation dependent p_f .

S1.1 Temperature-index model choice influence on calibrated parameter combinations (related to Sect. 3.1.1)

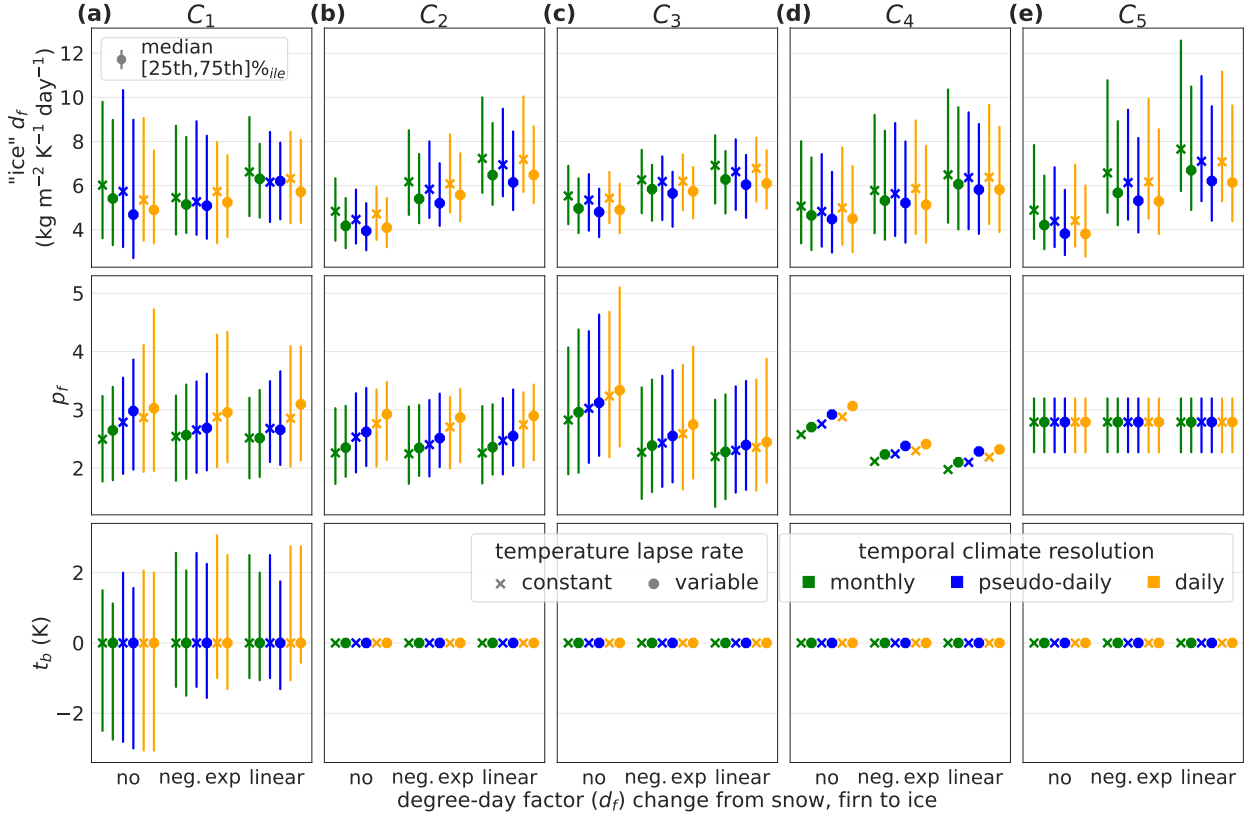


Figure S3: Calibrated model parameters for different temperature-index model (Table 1) and calibration (Table 2) options C_1 – C_5 . d_f stands for degree-day factor, p_f for precipitation factor, and t_b for temperature bias. The parameter distributions (median and interquartile range, 25%_{ile}–75%_{ile}) are shown for the 88 glaciers with enough in-situ observations to apply all calibration strategies.

In the main paper, we only shortly mentioned the temperature-index degree-day factor differences for calibration strategy C_5 (Fig. 1). Side remark: the unit of the degree-day factor in e.g. Huss and Hock (2015); Braithwaite (2008) is in $\text{mm K}^{-1} \text{day}^{-1}$. However, they actually mean $\text{mm w.e. K}^{-1} \text{day}^{-1}$ (personal communication).

Here, we provide additional details for calibration strategies C_1 – C_4 and always relate to Fig. S3:

S1.1.1 Temperature lapse rate choice

When allowed to vary, the precipitation factor is larger for the variable (weaker negative) lapse rates compared to the constant lapse rate. Following Fig. 4a, a smaller precipitation factor would be needed to match the observations if a lower degree-day factor is applied. Thus, the reversed relationship that results in lower degree-day factors for the variable lapse rates compared to the constant lapse rate is not a result of equifinality but a result of the higher air temperatures. The temperature bias differences between constant and variable temperature lapse rate (same for the temporal climate data choice) in C_1 are not systematic (Fig. SS3a) and balance out differences from the other two parameters.

S1.1.2 Temporal climate resolution choice

For the daily choice, the additional daily distinction between snow and rain likely results in a slightly larger degree-day factor compared to the pseudo-daily choice.

In all calibration strategies with variable precipitation factors (C_1 – C_4 , Fig. SS3a–d), the theoretically decreased solid precipitation for the daily choice is balanced out by a larger precipitation factor to match the average winter MB (Fig. SS3b), the interannual MB variability (Fig. SS3c) or both (Fig. SS3a).

S1.1.3 Surface-type distinction choice

When only matching the winter MB and not applying any temperature bias (C_2), the precipitation factor is almost the same for the three surface-type distinction choices (Fig. S3b). Winter MB depends much more on the precipitation factor than the degree-day factor; thus, the surface-type distinction makes little difference. When matching interannual MB variability (C_3), a temperature-index model where the degree-day factor changes from snow to firn or ice needs a smaller precipitation factor than one without (Fig. S3c). With surface-type distinction, positive MB anomalies from large (solid) precipitation years are enhanced by the lower snow degree-day factor, and negative MB anomalies are enhanced by using the higher firn or ice degree-day factor. Consequently, if a calibration strategy uses the same precipitation factor, the interannual MB variability will be larger for models including surface-type distinction.

When having three free parameters (C_1), neither precipitation nor degree-day factor changes consistently between the surface-type distinction choices (Fig. S3a). However, the temperature bias changes, which has a similar effect as a higher degree-day factor. A positive temperature bias is applied to balance out otherwise decreased melt for model choices with surface-type distinction, and a negative temperature bias is applied for those without surface-type distinction (Fig. S3a). Again, this is not a result of equifinality but reflects the parameter combinations which better match all observed variables.

S1.2 Supplemental Figures of temperature-index model choice and calibration strategy performance (related to Sect. 3.1.3 and Sect. 3.2.2)

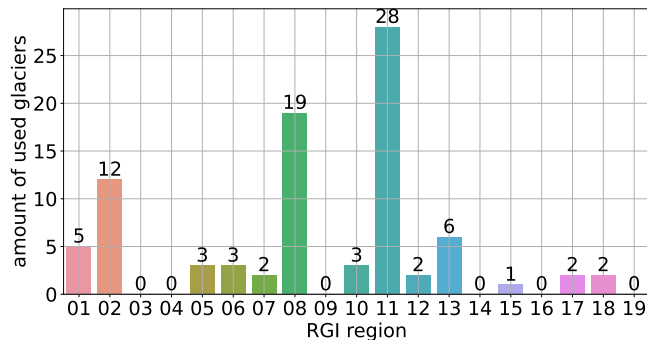


Figure S4: Amount of glaciers per RGI region that could be calibrated for all calibration and temperature-index model options (in total 88 glaciers). That means the glaciers need to have both sufficient winter MB and annual MB measurements available, as well as fitting parameter combinations for all options.

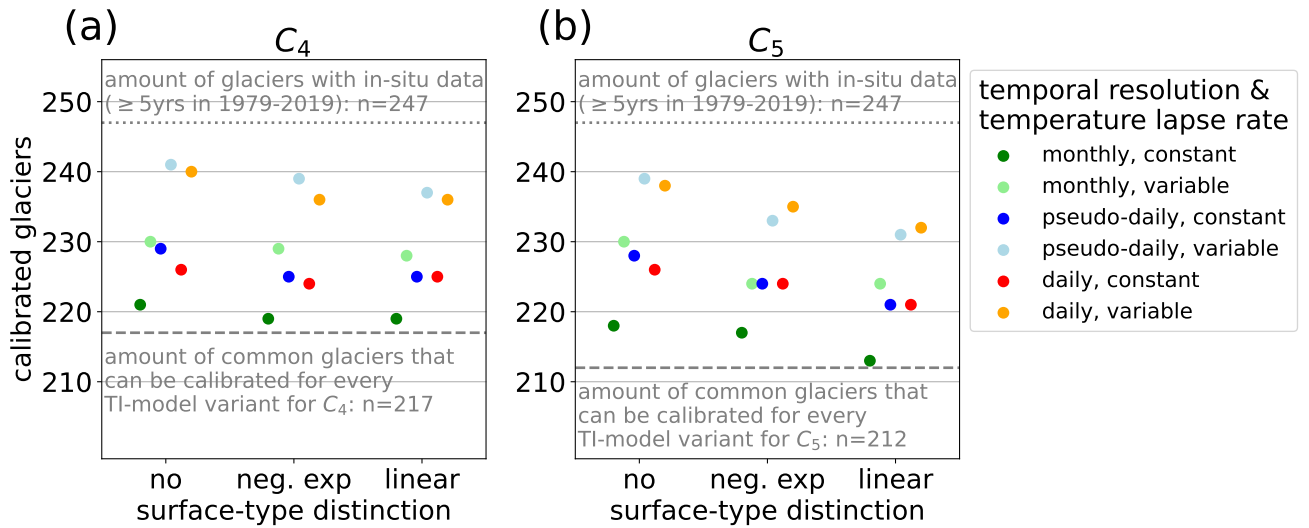


Figure S5: Amount of glaciers per temperature-index (TI) model choices that could be calibrated for calibration strategy (a) C_4 and (b) C_5 .

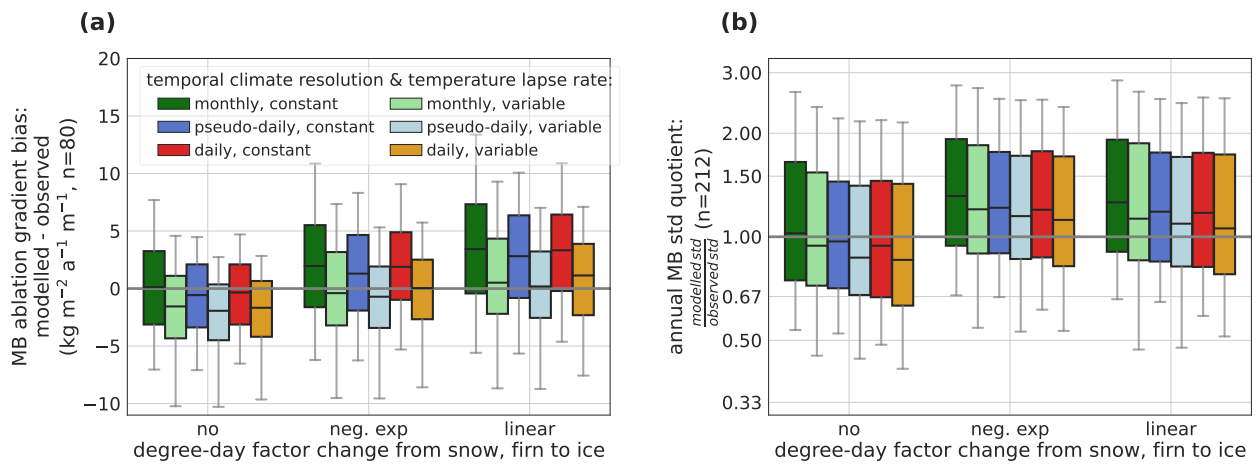


Figure S6: Performance of temperature-index model choices using different measures from independent observations and calibration strategy C_5 . In (a), the difference between modelled and observed mean MB gradient below the equilibrium line altitude (ELA) and in (b), the standard deviation quotient between modelled and observed interannual MB variability is shown. Distributions represented by the 5%_{ile}, 25%_{ile}, 50%_{ile} (median), 75%_{ile} and the 95%_{ile}.

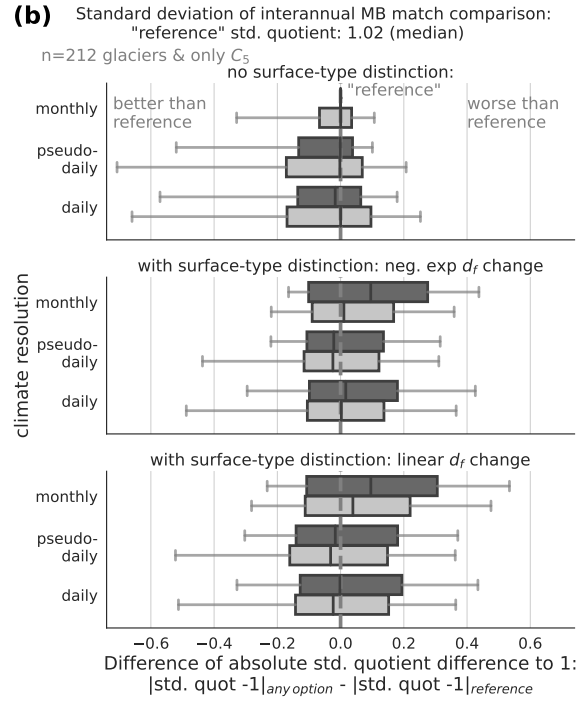
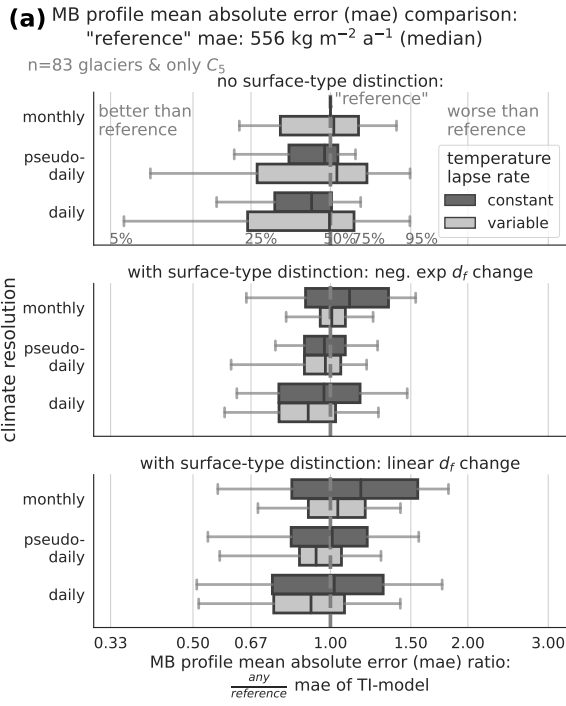


Figure S7: Performance comparison of temperature-index (TI) models for different measures from independent observations for calibration strategy C_5 . In (a), the ratio of MB profile mean absolute errors (mae) between observed and modelled mean MB profile over the observation years is shown for 83 glaciers. As we do not want to set too much weight on the wider snow or firn-covered accumulation area where uncertainties are larger, we compute the mae of the altitudinal bands without weighting for the glacier width. To compare the performance between different TI models, we divide the mae of every choice through the reference model choice. In (b), differences in the absolute std. quotients to one (i.e., a measure of how well the interannual MB is matched) are shown for 212 glaciers. d_f stands for degree-day factor. Distributions represented by the 5%_{ile}, 25%_{ile}, 50%_{ile} (median), 75%_{ile} and the 95%_{ile}. A distribution shift to the right means, for each measure, that this option matches the validation measure worse than the reference model. The differences in the mean MB gradient absolute bias below the equilibrium line altitude are shown in Fig. 3a.

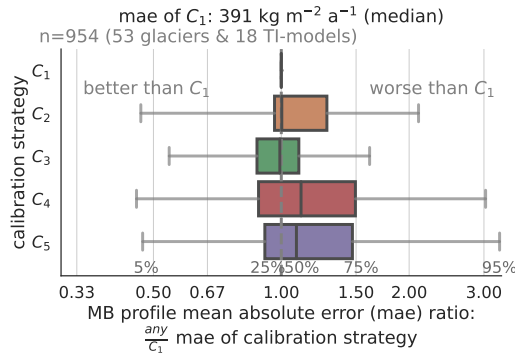


Figure S8: Performance comparison of calibration strategies: Same as Fig. 3b, but looking into the MB profile mean absolute error (mae) ratio (explained in caption of Fig. S7).

S1.3 Supplemental Figures of the influence of equifinality on the temperature-index model output (related to Sect. 3.2.1)

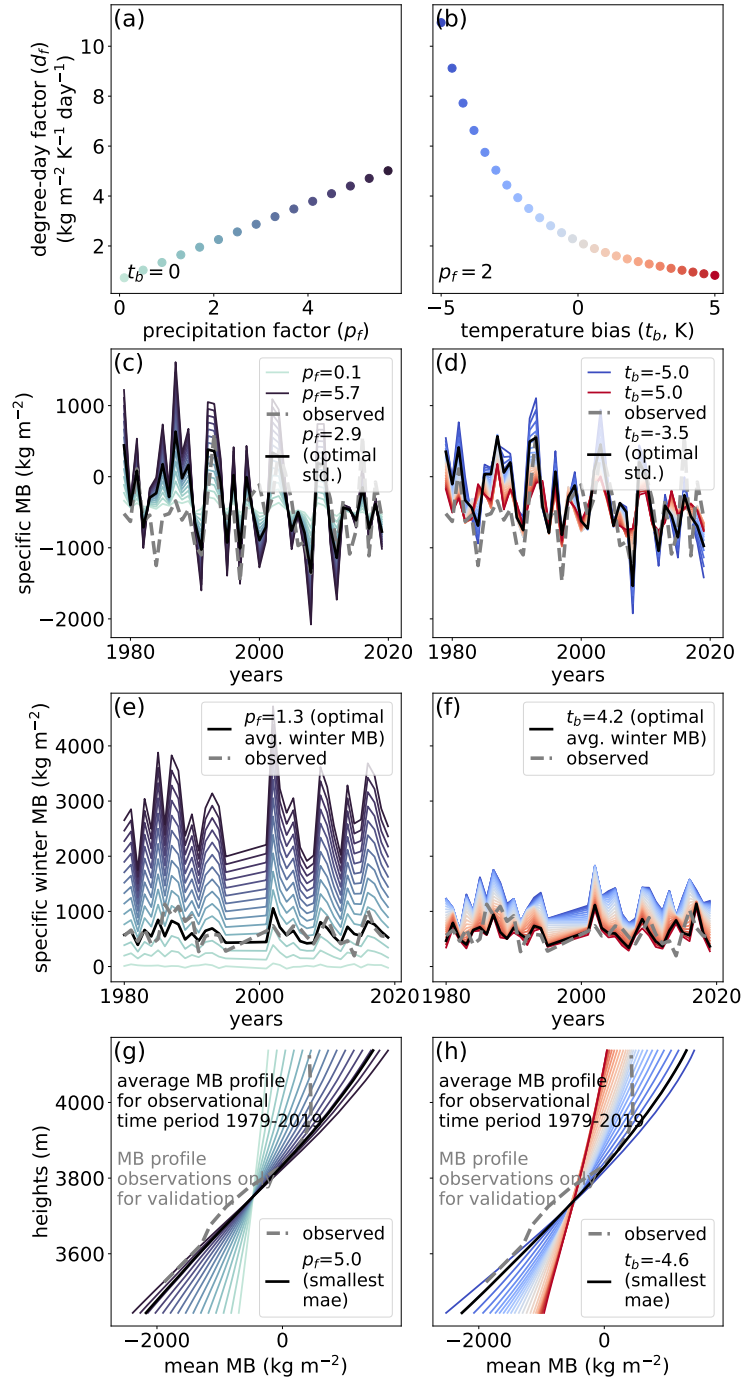


Figure S9: **Same as Fig. 4 but for RGI60-13.08624:** Influence of downscaling model parameters for RGI60-13.08624 on the calibrated (a, b) degree-day factor (d_f) to match the geodetic observations and on the resulting (c, d) interannual MB variability, (e, f) average winter MB and (g, h) mean elevation-dependent MB profiles (using the reference model option). Left plots (a, c, e, g) show varying precipitation factors (p_f) with temperature bias (t_b) set to zero, while right plots (b, d, f, h) show varying t_b with p_f set to two. Colorbar in (c–h) based on (a, b). std stands for standard deviation, mae for mean absolute error. Each d_f , p_f , and t_b combination matches the geodetic mean MB, and the combinations that best match in-situ observations are indicated. Modelled estimates only shown for years with observational data.

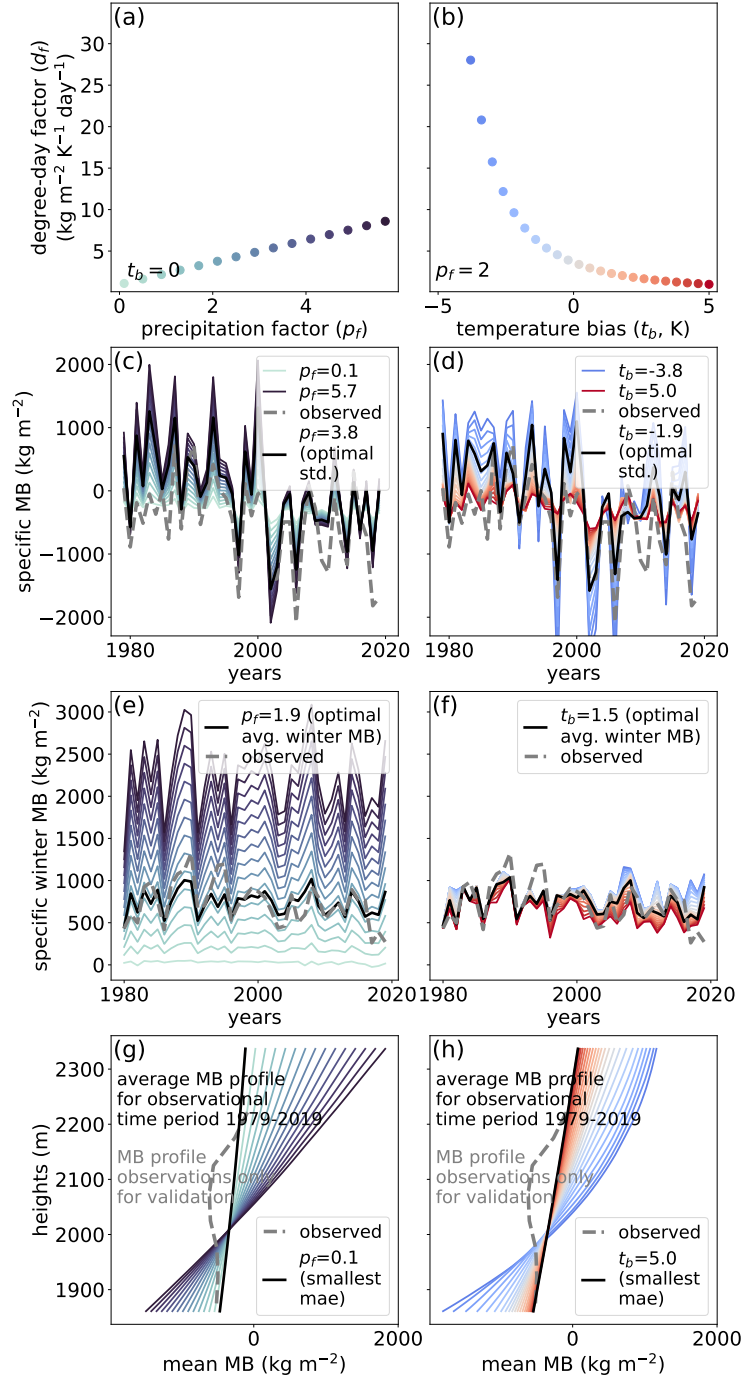


Figure S10: **Same as Fig. 4 but for RGI60-08.00987:** Influence of downscaling model parameters for RGI60-08.00987 on the calibrated (a, b) degree-day factor (d_f) to match the geodetic observations and on the resulting (c, d) interannual MB variability, (e, f) average winter MB and (g, h) mean elevation-dependent MB profiles (using the reference model option). Left plots (a, c, e, g) show varying precipitation factors (p_f) with temperature bias (t_b) set to zero, while right plots (b, d, f, h) show varying t_b with p_f set to two. Colorbar in (c–h) based on (a, b). std stands for standard deviation, mae for mean absolute error. Each d_f , p_f , and t_b combination matches the geodetic mean MB, and the combinations that best match in-situ observations are indicated. Modelled estimates only shown for years with observational data.

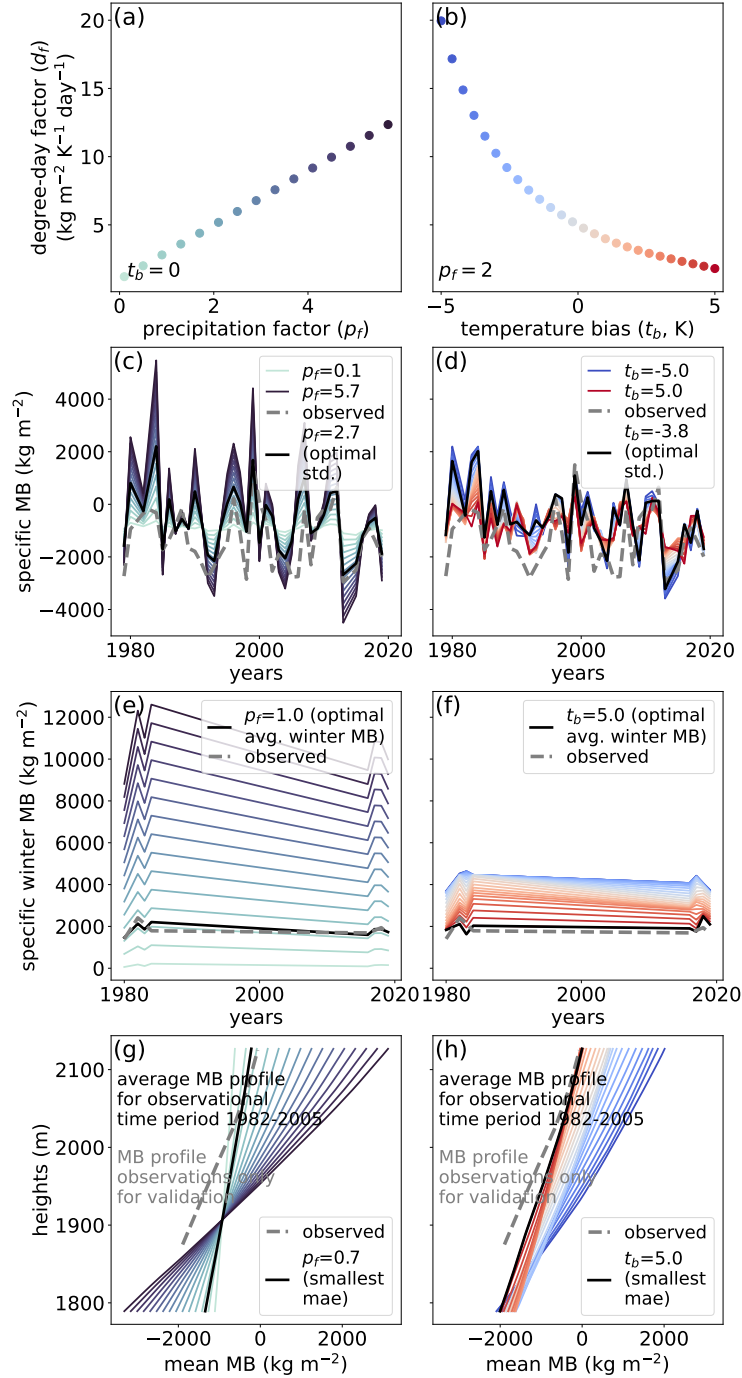


Figure S11: **Same as Fig. 4 but for RGI60-02.00377:** Influence of downscaling model parameters for RGI60-02.00377 on the calibrated (a, b) degree-day factor (d_f) to match the geodetic observations and on the resulting (c, d) interannual MB variability, (e, f) average winter MB and (g, h) mean elevation-dependent MB profiles (using the reference model option). Left plots (a, c, e, g) show varying precipitation factors (p_f) with temperature bias (t_b) set to zero, while right plots (b, d, f, h) show varying t_b with p_f set to two. Colorbar in (c–h) based on (a, b). std stands for standard deviation, mae for mean absolute error. Each d_f , p_f , and t_b combination matches the geodetic mean MB, and the combinations that best match in-situ observations are indicated. Modelled estimates only shown for years with observational data.

S2 Supplemental Figures of volume projections (related to Sect. 4)

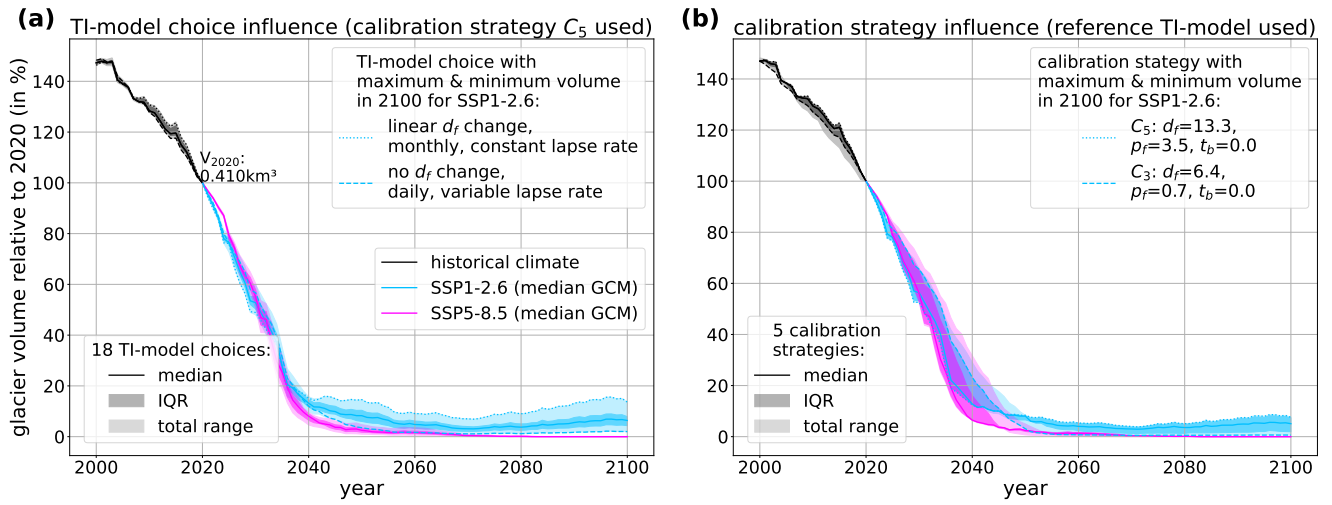


Figure S12: **Same as Fig. 5 but for Hintereisferner glacier (RGI60-11.00897):** Hintereisferner glacier volume projections (2000–2100) for two SSP scenarios. We show the median, interquartile range (25%ile–75%ile, IQR) and total range resulting from **(a)** temperature-index (TI-) model choices using C_5 and **(b)** calibration strategies using the reference model. d_f stands for degree-day factor, p_f for precipitation factor, and t_b for temperature bias. We use the median volume from five GCMs. Fig. 5 shows the same for the Aletsch glacier.

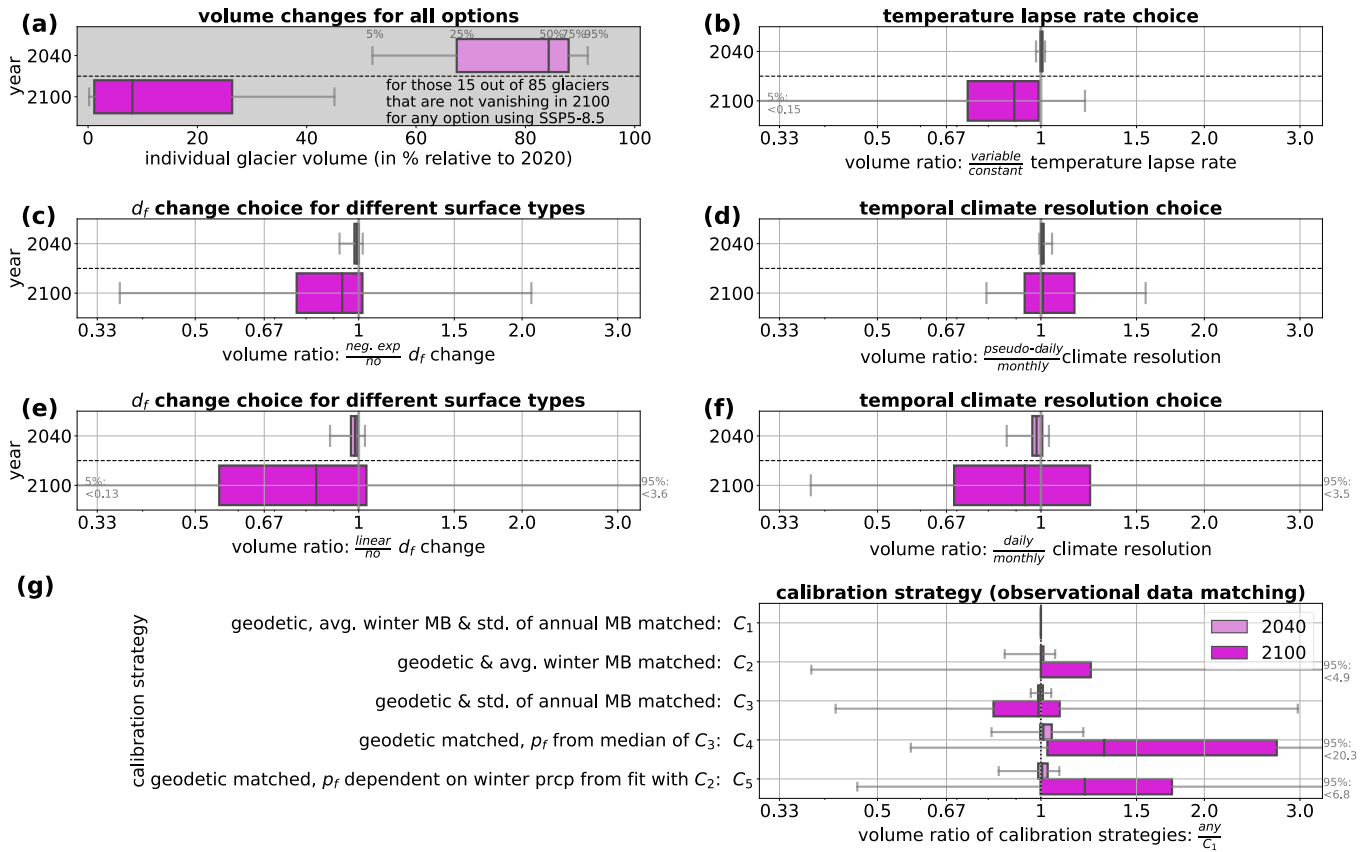


Figure S13: Same as Fig. 6 but for SSP5-8.5: (a) Individual glacier volume changes in 2040 and 2100 for 15 glaciers that could be calibrated on all options and still exist in 2100 under the SSP5-8.5 scenario. Individual glacier volume ratios for (b–f) temperature-index model choice and (g) calibration strategy. Distributions represented by the 5%_{ile}, 25%_{ile}, 50%_{ile} (median), 75%_{ile} and the 95%_{ile}. A rightward (leftward) distribution shift indicates larger (smaller) glacier volume compared to the reference option. (a) Volume changes are estimated from all 15 glaciers, 3 · 3 · 2 temperature-index model and 5 calibration options, volume ratios respectively by (b) 15 · (3 · 3) · 5, (c–f) 15 · (3 · 2) · 5, and (g) 15 · (3 · 3 · 2) glaciers and options. We use the median volume from five GCMs. See Fig. 6 for SSP1-2.6.

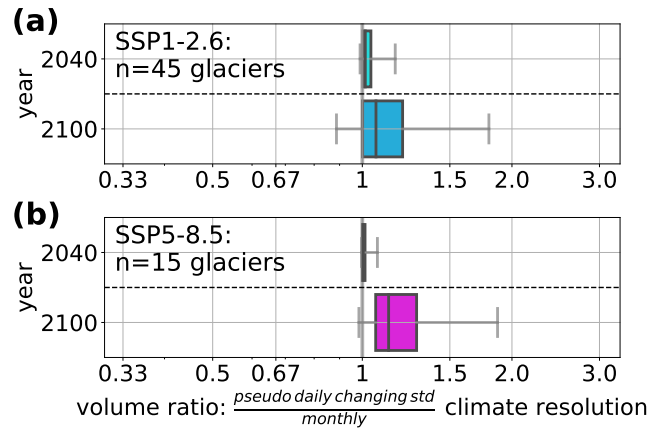


Figure S14: Additional subplot of (a) Fig. 6 and (b) Fig. S13 by comparing volume projections of another temporal climate resolution variant. “pseudo-daily changing std” is a choice where the applied daily temperature standard deviation is derived from the actual daily W5E5 and future GCMs instead of using a seasonally different but interannually constant standard deviation as used in the temperature-index model choice “pseudo-daily”. Distributions represented by the 5%_{ile}, 25%_{ile}, 50%_{ile} (median), 75%_{ile} and the 95%_{ile}. In 2100, using the “pseudo-daily changing std” compared to the monthly choice results in a larger projected glacier volume for more than 75% of the glaciers.

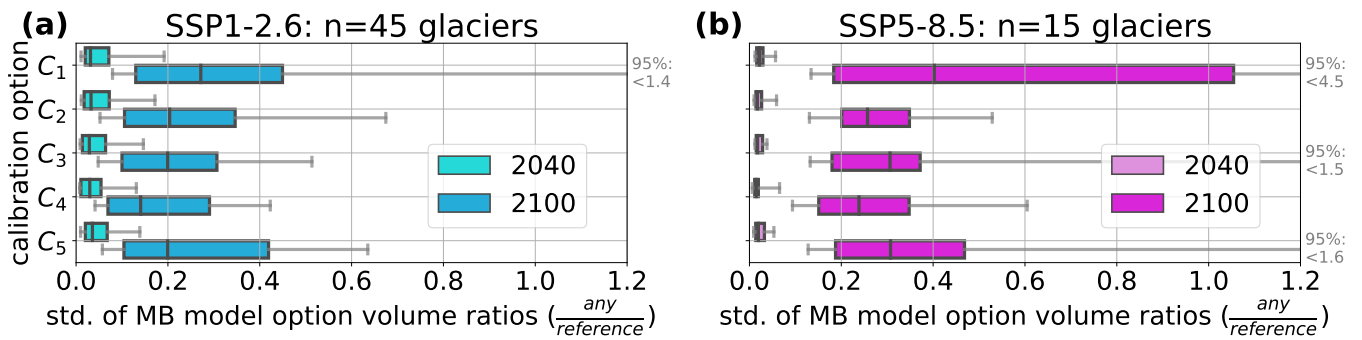


Figure S15: Standard deviation (std) of temperature-index model choice volume ratios for any versus the reference model for the different calibration strategies (see Table 2) in 2040 and 2100. In (a), the distribution from the common running and still in 2100 existing glaciers for SSP1-2.6 and in (b), respectively, for SSP5-8.5 are shown. The distribution of the standard deviation of the temperature-index model type volume ratios (for each glacier one std) is used here to compare how much the temperature-index model choices vary for each calibration strategy.

S3 Supplemental Figures of runoff projections (related to Sect. 4)

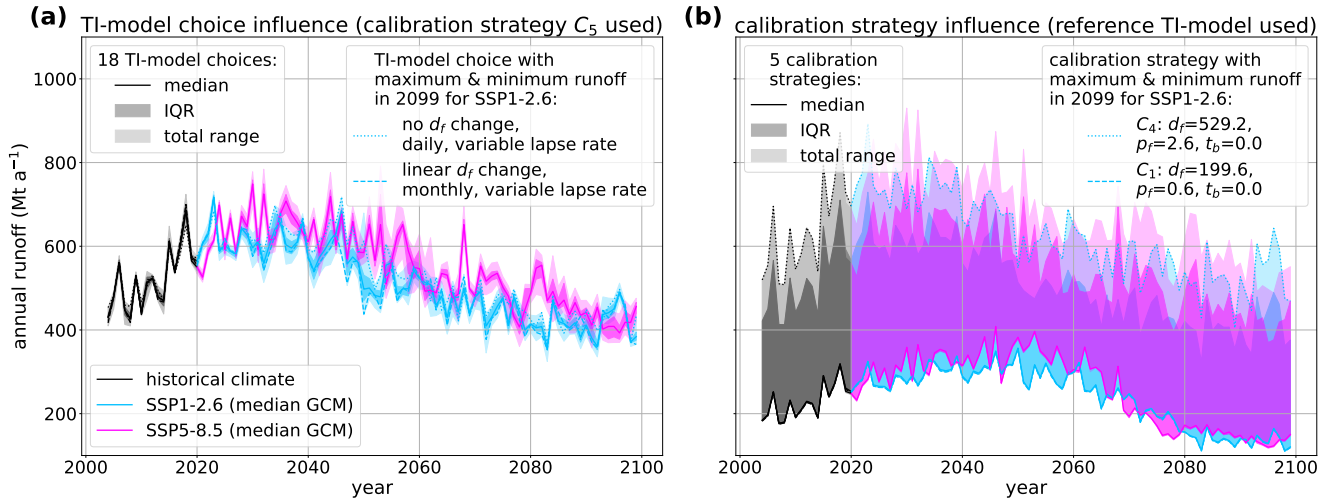


Figure S16: Aletsch glacier (RGI60-11.01450) projections for the annual runoff. We show the median, interquartile range (25%ile–75%ile, IQR) and total range resulting from **(a)** temperature-index (TI-) model choices using C_5 and **(b)** calibration strategies using the reference model. For this glacier, in **(b)**, the calibrated parameters and thus projections for C_1 , C_2 and C_5 are very similar. d_f stands for degree-day factor, p_f for precipitation factor, and t_b for temperature bias. The runoff estimates correspond to the median runoff from the five GCMs.

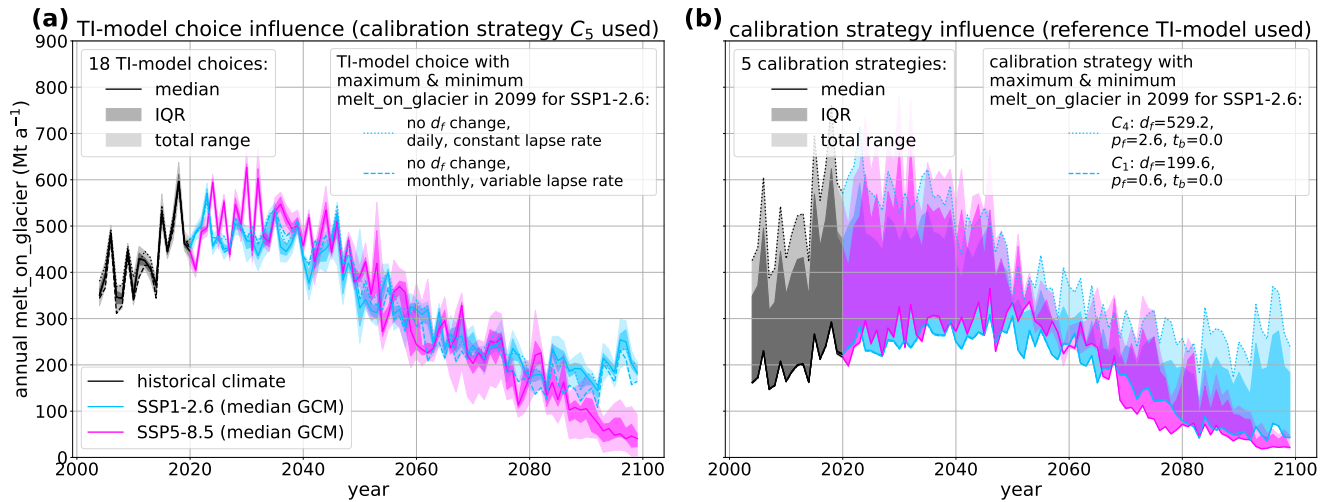


Figure S17: Aletsch glacier (RGI60-11.01450) projections for the melt on glacier contribution to the annual runoff (same structure as in Fig. S16). The melt on glacier estimates correspond to the median from the five GCMs.

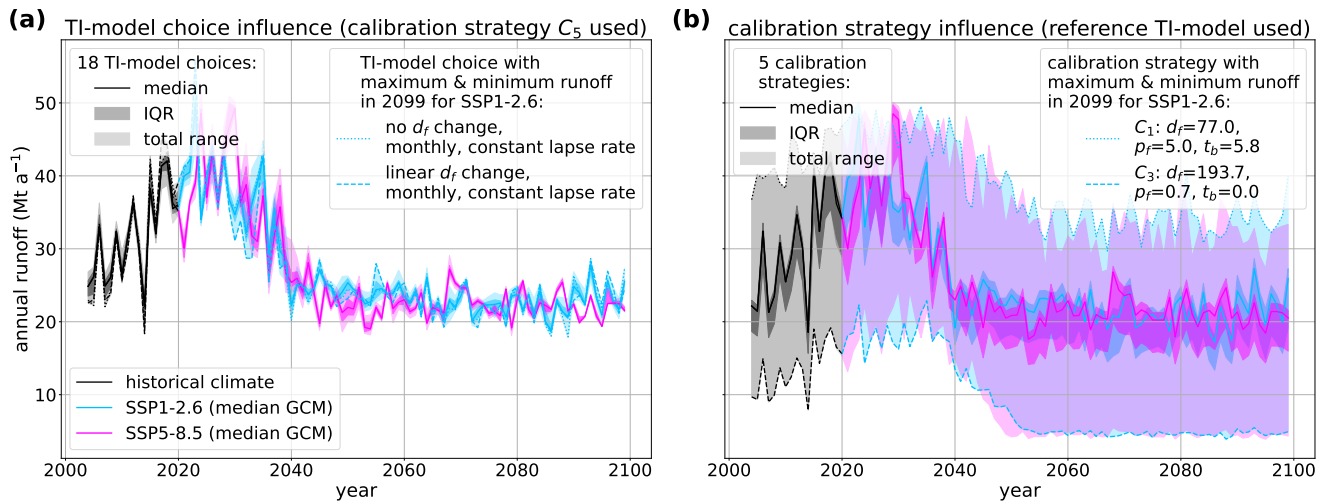


Figure S18: Hintereisferner glacier (RGI60-11.00897) projections for the annual runoff (same structure as in Fig. S16). The runoff estimates correspond to the median from the five GCMs.

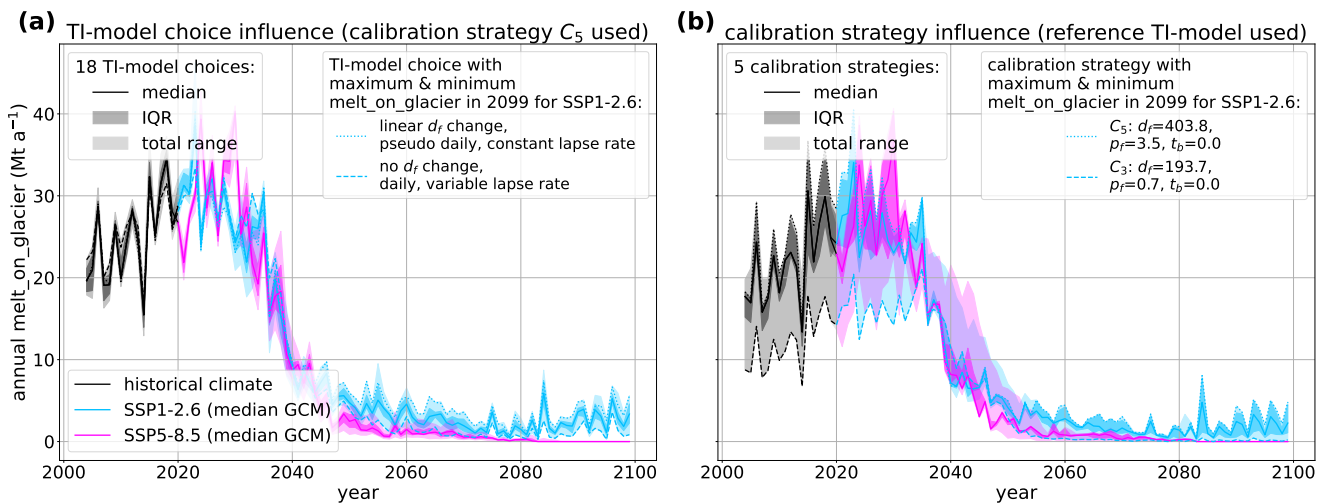


Figure S19: Hintereisferner glacier (RGI60-11.00897) projections for the melt on glacier contribution to the annual runoff (same structure as in Fig. S16). The melt on glacier estimates correspond to the median from the five GCMs.

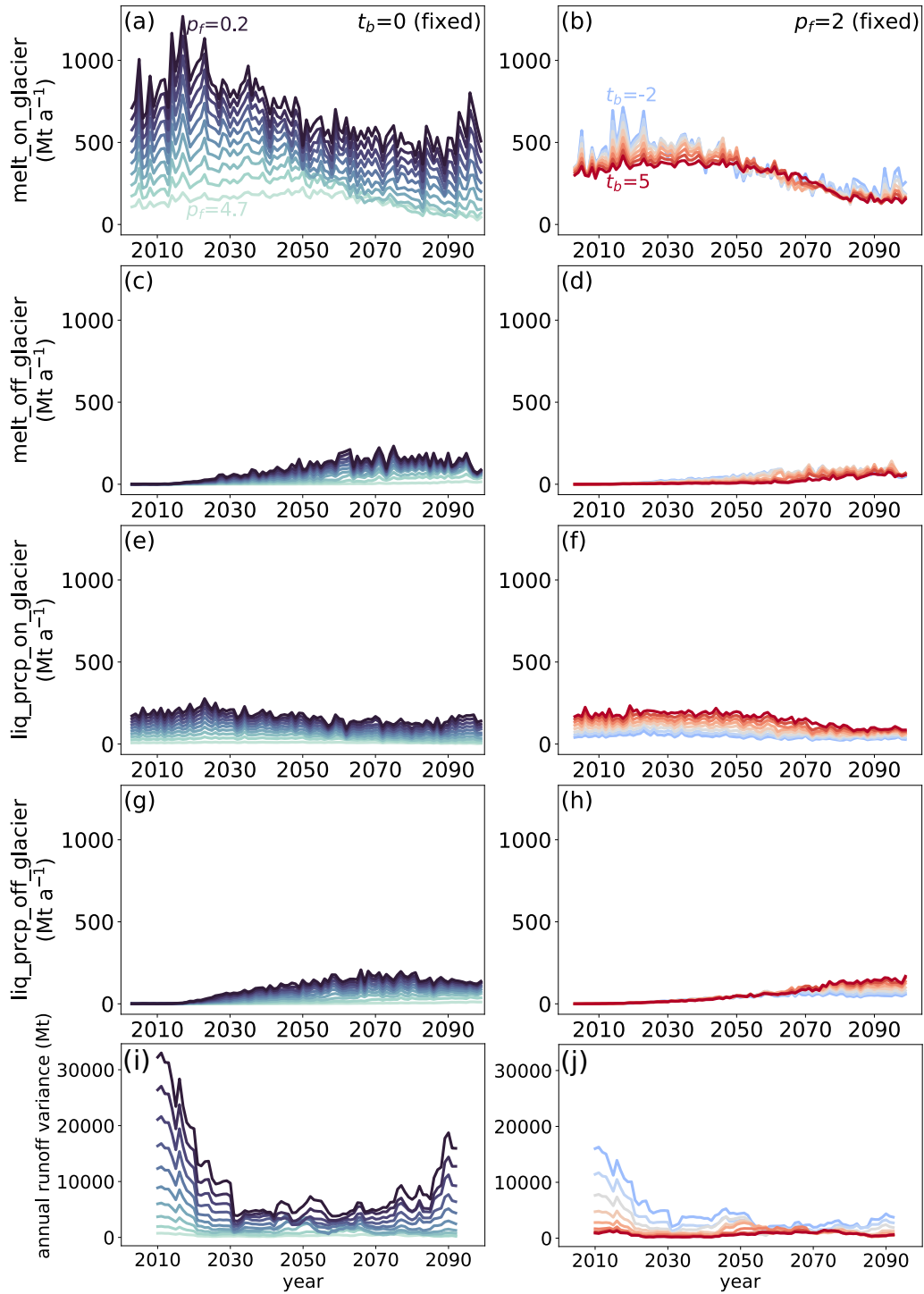


Figure S20: **Additional subplots of Fig. 7 with (a–h) the four different runoff components of OGGM and (i, j) the annual runoff variance for the Aletsch glacier under SSP1-2.6:** Influence of equifinality on (a, b) melt on glacier, (c, d) melt off glacier, (e, g) liquid precipitation on glacier and (g, h) liquid precipitation off glacier projections. The “off”-glacier parts are coming from the former glacier area at the RGI date. Thus, the “on”-glacier components are dominant over the first decades while the “off”-glacier influence increases as the glacier melts away. The colors indicate the precipitation factor (p_f) or temperature bias (t_b) as presented in (a, b) or in Fig. 7 (e, f). In (i, j), the annual runoff variance is displayed as a 15-year rolling average. For each p_f or t_b , a degree-day factor was calibrated to match the same average geodetic MB. On the left, t_b is set to zero and p_f is varied while on the right, p_f is set to 2 and t_b is varied. Projections are median estimates from five GCMs using the reference model.

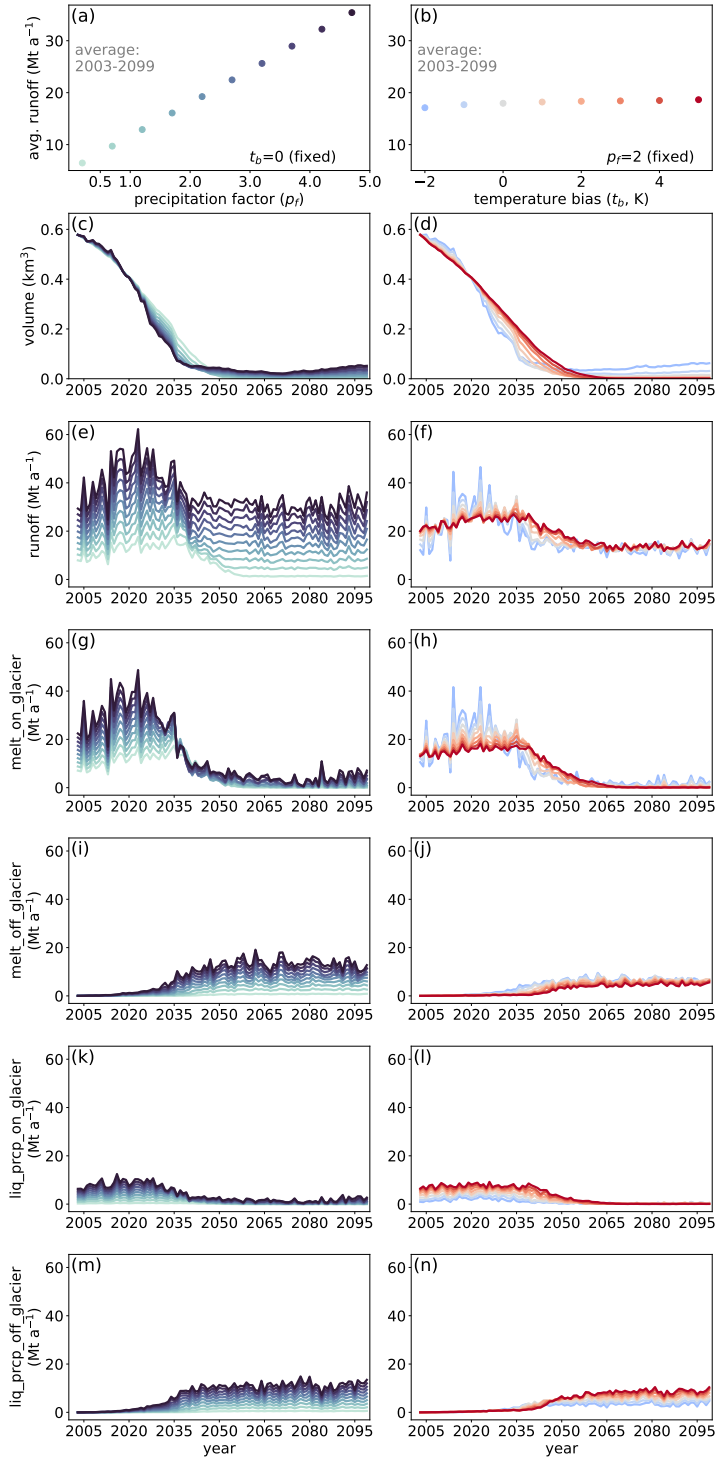


Figure S21: **Same as Fig. 7 and Fig. S20 together, but for Hintereisferner glacier:** Influence of equifinality on **(a, b)** volume and **(c, d)** runoff projections for the Hintereisferner glacier under SSP1-2.6. The projections of the four different runoff components (**(g, h)** melt on glacier, **(i, j)** melt off glacier, **(k, l)** liquid precipitation on glacier and **(k, l)** liquid precipitation off glacier) are also shown. The colors indicate the precipitation factor (p_f) or temperature bias (t_b) as presented in **(e, f)**, which shows the relation between p_f or t_b and average annual runoff. For each p_f or t_b , a degree-day factor was calibrated to match the same average geodetic MB. On the left, **(a, c, e, g, j, k, m)**, t_b is set to zero and p_f is varied while on the right, **(b, d, f, h, j, l, n)**, p_f is set to 2 and t_b is varied. Projections are median estimates from five GCMs using the reference model.

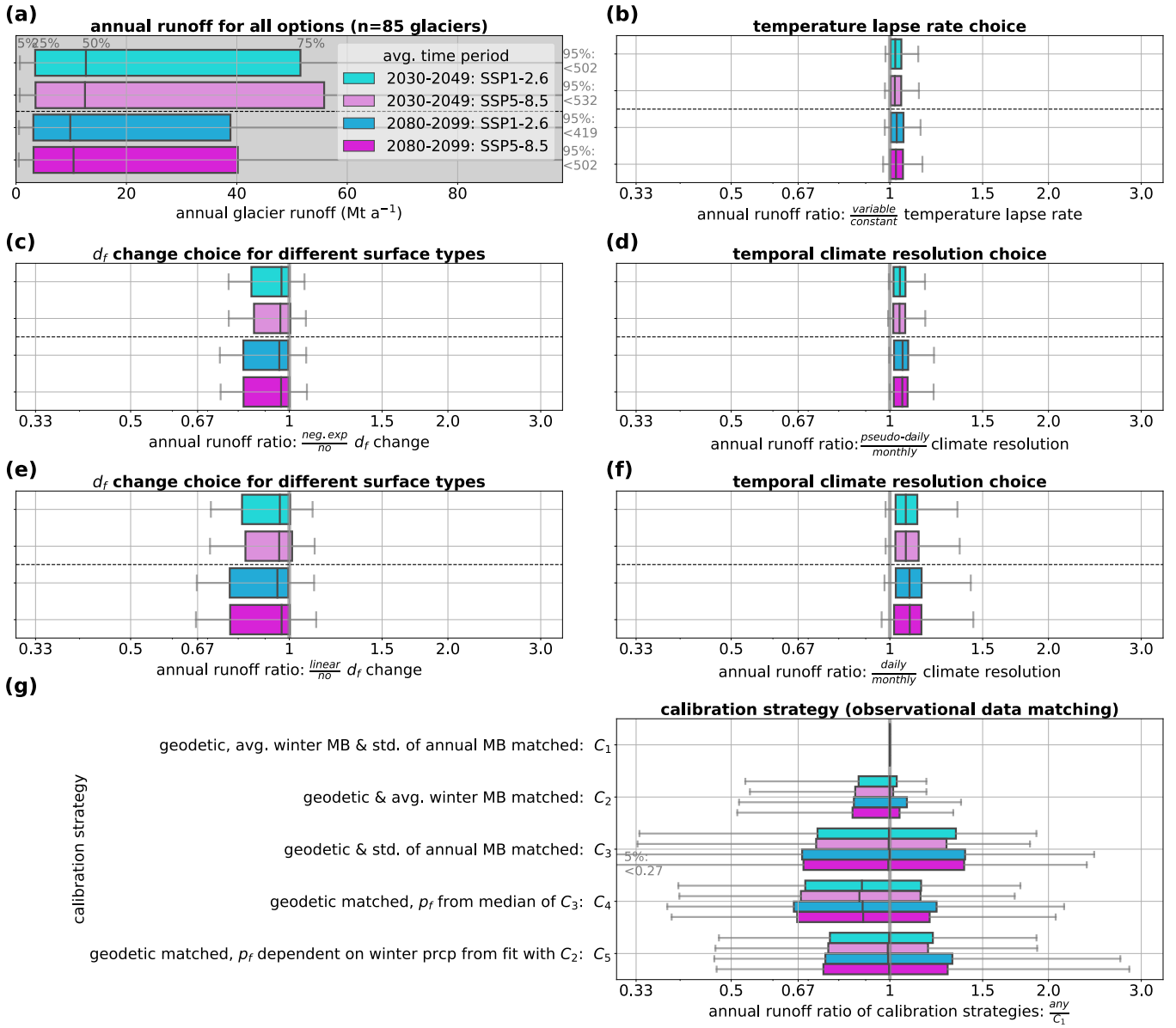


Figure S22: Glacier runoff projections for SSP1-2.6 and SSP5-8.5 for the 85 glaciers that could be calibrated and simulated on all options. The figure is similarly constructed as Fig. 6 and Fig. S13, but here the fixed-gauge runoff instead of the volume is shown. Note that many glaciers do not exist any more in 2100 (e.g., around half of them for SSP1-2.6) but the runoff of the former glacierized area is included as we account for the off-glacier runoff.

(a) Individual annual glacier runoff averaged over 2030–2049 and 2080–2099 for the 85 glaciers. Individual annual glacier runoff ratios for (b–f) temperature-index model choice and (g) calibration strategy. Distributions represented by the 5%ile, 25%ile, 50%ile (median), 75%ile and the 95%ile. A rightward (leftward) distribution shift indicates larger (smaller) annual glacier runoff compared to the reference option. (a) Runoff is estimated from all 85 glaciers, 3 · 3 · 2 temperature-index model and 5 calibration options, volume ratios respectively by (b) 85 · (3 · 3) · 5, (c–f) 85 · (3 · 2) · 5, and (g) 85 · (3 · 3 · 2) glaciers and options. We use the median volume from five GCMs.

S4 Supplemental Material for the discussion

S4.1 Comparison of other studies discussing the added value of more observations for the calibration (related to Sect. 5.1.4)

The climate dataset choice can have a similar influence on the model performance as the precipitation factor choice, i.e., both a climate dataset with larger winter precipitation (Compagno and others, 2021) or a larger precipitation factor (Fig. 4e) result in a larger winter MB. Using 16 regionally fixed parameter sets of precipitation factors and degree-day factors and only changing the temperature bias on a glacier-per-glacier level resulted in poorer model performance in Huss and Hock (2015) compared to their reference parameter calibration strategy (i.e., varying first the precipitation factor in a specific range, then, if necessary, the degree-day factor within a range, followed by the temperature bias) for Alpine glaciers. When optimising six MB model parameters to geodetic, point stake data and transient snowline retreat, the resulting parameter combination ensemble showed only little spread over historical MB estimates on a single glacier in Geck and others (2021). This limited impact of equifinality can be attributed to available higher temporally and spatially resolved MB observations during calibration, as well as narrower parameter ranges due to the use of weather station data to drive their enhanced temperature-index model.

References

- Braithwaite RJ (2008) Temperature and precipitation climate at the equilibrium-line altitude of glaciers expressed by the degree-day factor for melting snow. *Journal of Glaciology*, **54**(186), 437–444 (doi: 10.3189/002214308785836968)
- Compagno L, Zekollari H, Huss M and Farinotti D (2021) Limited impact of climate forcing products on future glacier evolution in Scandinavia and Iceland. *Journal of Glaciology*, **67**(264), 727–743 (doi: 10.1017/jog.2021.24)
- Farinotti D, Huss M, Fürst JJ, Landmann J, Machguth H, Maussion F and Pandit A (2019) A consensus estimate for the ice thickness distribution of all glaciers on Earth. *Nature Geoscience*, **12**(3), 168–173 (doi: 10.1038/s41561-019-0300-3)
- Geck J, Hock R, Loso MG, Ostman J and Dial R (2021) Modeling the impacts of climate change on mass balance and discharge of Eklutna Glacier, Alaska, 1985-2019. *Journal of Glaciology*, **67**(265), 909–920 (doi: 10.1017/jog.2021.41)
- Huss M and Hock R (2015) A new model for global glacier change and sea-level rise. *Frontiers in Earth Science*, **3**(September), 1–22 (doi: 10.3389/feart.2015.00054)